4 Lattice considerations

D. Einfeld

4.1 Introduction

One of the first proposals for the lattice design of a *diffraction-limited light source* was produced in the early 1990s [4.1−4.5]. At that time the new 3rd generation light sources ALS, ESRF, and ELETTRA were commissioned in record time. All three machines reached their target specifications without any significant beam-dynamic problems and have operated reliably ever since. The successful commissioning results built confidence in the ability to operate storage rings with horizontal emittances an order of magnitude lower, in the 0.5 nmrad range. With a coupling of 1%, the vertical emittance would be of the order of 5 pmrad. The original calculations having been performed over 20 years ago, the new MAX IV [4.6] facility will be the first SRL to implement a sub-nmrad variant of this design, and other proposed machines are following the multi-bend achromat (MBA) concept.

One of the most important factors in synchrotron radiation research is photon beam brilliance, which in storage rings is determined by the electron beam emittance and the coupling between the horizontal and vertical planes. Even in the limit of zero beam emittance, however, the phase space of the radiation emission from an undulator is itself finite due to diffraction effects at the source. For single-mode photon emission, the corresponding diffraction-limited 'emittance' of the photon beam is given by

$$\varepsilon(\text{phot}) \le \frac{\lambda}{4\pi} = 0.159\lambda = 98.66\ \text{pmrad} / (E_\gamma / \text{keV}), \tag{4.1}$$

where λ is the X-ray wavelength and E_γ is the photon energy in keV [4.7, 4.8]. For photon energies of 1, 5, and 10 keV, the corresponding beam emittance should be smaller than 100, 20, and 10 pmrad, respectively. Equation (4.1) has been much debated, and there is still no consensus that the factor of 4π in the denominator is numerically correct [4.8]. Nevertheless, a light source is referred to as 'diffraction-limited' when the electron beam emittance is less than that of the radiated photon beam at the desired X-ray wavelength.

By way of review, recall that the horizontal emittance of an electron storage ring beam is determined by a balance between two competing processes: 1) quantum excitation of betatron oscillations from photon emission according to Eq. (3.3) and 2) longitudinal re-acceleration within the radio-frequency (RF) cavities to bring the beam to the nominal energy E_0 again. The basic formula for calculating storage ring emittance, assuming isomagnetic bend magnets and no insertion devices, is summarized [4.9] as

$$\varepsilon = C_q \gamma_0^2 \frac{\langle H \rangle_{\text{mag}}}{J_x \rho}, \tag{4.2}$$

where $C_q = 3.841 \times 10^{-13}$ m is a constant, γ_0 is the relativistic Lorentz factor, J_x is the Robinson partition number evaluated for the horizontal plane, ρ is the dipole magnet bending radius, and $\langle H \rangle_{\text{mag}}$ is the average of H evaluated in the bending magnets,

$$\langle H \rangle = \frac{1}{2\pi\rho_0} \int \gamma\eta^2 + 2\alpha\eta\eta' + \beta\eta'^2 \, \text{d}s. \tag{4.3}$$

The definitions of $\alpha(s)$ and $\gamma(s)$ are

$$\alpha(s) = -\frac{1}{2}\beta'(s), \quad \gamma(s) = \frac{1+\alpha^2(s)}{\beta(s)}. \tag{4.4}$$

https://doi.org/10.23731/CYRM-2020-001.25

In Eqs. (4.3) and (4.4), α, β, and γ are the standard position-dependent Twiss parameters in the horizontal plane, and η and η' are the horizontal dispersion function and its first derivative, respectively. As a general rule, for low emittance one has to minimize the integral quantity $\langle H \rangle_{\text{mag}}$ to maintain sufficient straight-section free space for insertion devices and operate at sufficiently high beam energy to meet the spectral requirements of the user community.

4.2 Low-emittance lattice design

Referring again to Eq. (4.2), the horizontal beam emittance is seen to scale with the square of the beam energy, scale linearly with $\langle H \rangle_{\text{mag}}$, and be inversely proportional to the partition number J_x. For bending magnets with a pure dipole field, $J_x = 1$. Since the H-function is determined by the Twiss parameters and the dispersion in bending magnets, low emittance can be achieved if the beam sigma matrix and $\eta(s)$ have specifically controlled values within the bending magnets. For example the horizontal emittance can be analytically evaluated for two well-known cases: the first bend magnet of a flat-field *double-bend achromat* (DBA) lattice [4.10]; and the centre bend magnet of a flat-field *triple-bend achromat* (TBA) structure [4.11] (see Fig. 4.1).

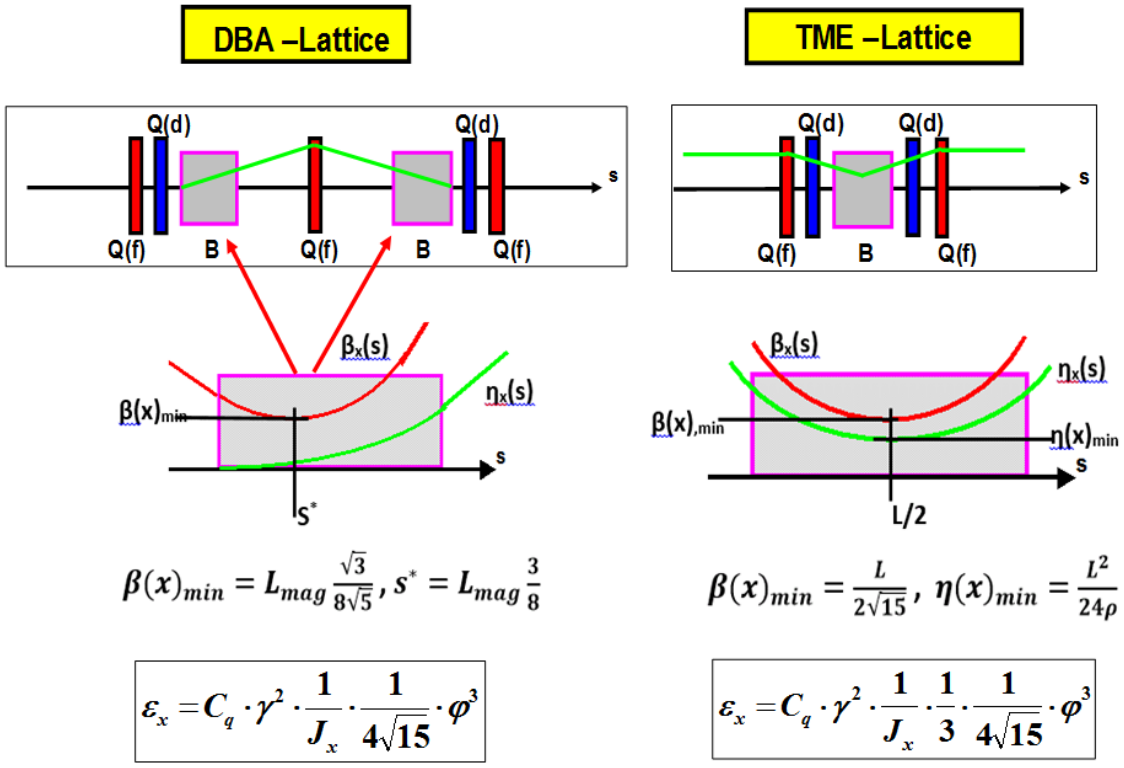

Fig. 4.1: The DBA lattice and TME structure to attain a minimum emittance

The *theoretical minimum emittance* (TME) of a storage ring beam can be attained only when both the horizontal beta function and the horizontal dispersion reach a minimum at the centre of the bending magnets. These conditions are met when $\beta_{\text{min}} = L/2\sqrt{15}$ and $\eta_{\text{min}} = L^2/(24\rho)$ [4.12, 4.13], yielding

$$\varepsilon(\text{TME}) = C_q \gamma_0^2 \frac{1}{J_x} \times \frac{1}{3} \times \frac{1}{4\sqrt{15}} \phi^3 = \frac{31.65\,\text{nm rad}}{J_x} \left(\frac{E}{\text{GeV}}\right)^2 \left(\frac{\phi}{\text{rad}}\right)^3 . \qquad (4.5)$$

According to Eq. (4.5), the TME is proportional to the third power of the dipole magnet deflection angle ϕ and the square of the electron energy. In practice, most conventional light sources operate with a horizontal emittance of two to five times the TME value.

The optimum emittance of a DBA lattice is a factor of 3 above TME (see Fig. 4.1). The horizontal partition number J_x is given by

$$J_x = 1 - D, \quad D = \frac{1}{2\pi\rho^2}\int \eta[1 - 2k\rho^2]ds\,, \tag{4.6}$$

where $k(s)$ is the normalized quadrupole gradient in the bending magnets. For bending magnets with a pure dipole field, $J_x = 1$. Vertical focusing in the bending magnets increases J_x to a maximum of 2, yielding a reduction in emittance of up to a factor of 2; however, the energy spread goes up and could have negative effects.

The introduction of damping wigglers serves to increase the radiated energy loss per turn, U_0, by an amount U_{Wi} [4.12, 4.13, 4.14], and to first approximation this decreases the emittance as follows:

$$\varepsilon_{\mathrm{Wi}} = \varepsilon_0 \frac{U_0}{U_0 + U_{\mathrm{Wi}}}\,, \tag{4.7}$$

$$U_0 = 88.46\ \mathrm{keV} \times \frac{\left(\frac{E}{\mathrm{GeV}}\right)^4}{\left(\frac{\rho}{\mathrm{m}}\right)}\,, \tag{4.8}$$

$$U_{\mathrm{Wi}} = 0.633\ \mathrm{keV} \times \left(\frac{L}{\mathrm{m}}\right)\left(\frac{E}{\mathrm{GeV}}\right)(B_{\mathrm{m}})^2\,. \tag{4.9}$$

In Eqs. (4.7)–(4.9), U_0 is the energy loss per turn in the bending magnets and U_{Wi} is that in the insertion devices.

To achieve low emittance in the storage ring, the following points should be considered.

(i) The number of magnets has to be large, which means using *multi-bend achromat* (MBA) cells with five or more bending magnets.

(ii) The outer bending magnets must be shorter by roughly a factor of 2.

(iii) The bending magnets should be of combined-function construction with vertical focusing to increase and maximize J_x. Combined-function bending magnets also have the advantage of yielding a compact machine design, and they can often increase separation of the beta functions at sextupole locations.

(iv) Damping wigglers can be installed to increase radiative energy loss per turn and therefore decrease emittance.

(v) Longitudinal-gradient bending magnets have the potential to further decrease emittance [4.14].

4.3 The synchrotron radiation brilliance

The brilliance is calculated according to

$$B = \frac{\dot{N}}{2\pi^2 \Sigma_x \Sigma_y \Sigma_{x'} \Sigma_{y'}}\,, \tag{4.10}$$

where $\dot{N}$ is the photon flux in the central cone, which depends only on the number of periods, the beam current, and a function independent of the machine parameters. Hence, for a given insertion device, the flux for each harmonic is the same, and the energy at which each harmonic is located depends on the energy of the machine, as shown in Eqs. (4.11) and (4.12); K is the so-called deflection parameter:

$$E_r(n) = \frac{0.949\ \text{keV} \times \left(\frac{E}{\text{GeV}}\right)^2 \times n}{\left(\frac{\lambda_u}{\text{cm}}\right)\left(1+\frac{K^2}{2}\right)}\ , \tag{4.11}$$

$$K = 0.934 \times \left(\frac{B_0}{T}\right)\left(\frac{\lambda_u}{\text{cm}}\right). \tag{4.12}$$

Therefore, the differences between the brilliances of different lattices will come from the factor

$$\frac{1}{\Sigma_x \Sigma_y \Sigma_{x'} \Sigma_{y'}}\ . \tag{4.13}$$

The denominator in (4.13) corresponds to the multiplication of convoluted sizes of electron and photon beams, i.e.,

$$\Sigma_x = \sqrt{\sigma_x^2 + \sigma_r^2}\ , \quad \Sigma_y = \sqrt{\sigma_y^2 + \sigma_r^2}\ , \quad \Sigma_{x'} = \sqrt{\sigma_{x'}^2 + \sigma_{r'}^2}\ , \quad \Sigma_{y'} = \sqrt{\sigma_{y'}^2 + \sigma_{r'}^2}\ . \tag{4.14}$$

The beam sizes and divergences $\sigma_x, \sigma_y, \sigma_{x'}$ and $\sigma_{y'}$ depend on machine parameters, the emittance ε, and the beta functions β_x and β_y. If the dispersion function at the position of the undulator is zero, $\sigma_x, \sigma_y, \sigma_x'$ and σ_y' are given by

$$\sigma_x = \sqrt{\varepsilon_x \beta_x}\ , \quad \sigma_y = \sqrt{\varepsilon_y \beta_y}\ , \quad \sigma_x' = \sqrt{\varepsilon_x / \beta_x}\ , \quad \sigma_y' = \sqrt{\varepsilon_y / \beta_y}\ . \tag{4.15}$$

The photon size and dispersion σ_r and $\sigma_{r'}$ for each harmonic depend on the length of the undulator L and the characteristic undulator wavelength λ [4.8]:

$$\sigma_r = \frac{1}{\sqrt{2}\pi}\sqrt{\lambda L}\ , \quad \sigma_{r'} = \frac{1}{\sqrt{2}}\sqrt{\frac{\lambda}{L}}\ , \quad \lambda = \frac{l_u}{2\pi\gamma^2}\left(1+\frac{K^2}{2}\right). \tag{4.16}$$

Here K is the deflection parameter, L is the length of the undulator, l_u is the undulator period, and n is the harmonic number. According to the investigations by Kim [4.15], the dimension of the photon source size differs by a factor of ½. The machine energy is given by the factor $1/\gamma^2$, so higher machine energy means lower wavelength (or higher photon energy). Therefore photon size decreases with machine energy, and hence brilliance, which depends on the photon size, increases with machine energy.

The cross-section and divergence of the undulator radiation are presented in Figs. 4.2 and 4.3. The radiation cross-section $\sigma(r)$ goes from 2 μm at 4 keV to 0.6 μm at 36 keV. The horizontal cross-section $\sigma(x)$ for the different lattices goes from 40 to 70 μm; hence the radiation cross-section has only a marginal influence on the brilliance. What is important is the horizontal beam cross-section σ_x, given by the emittance and the beta function. According to the data given for the vertical direction, the radiation cross-section has a non-negligible effect on the brilliance.

It is completely different for the influence of the radiation divergence σ_r' on the brilliance. In the horizontal direction the two contributions are approximately equal, but in the vertical direction the divergence σ_r' of the undulator radiation determines the brilliance. Hence the beta function in the vertical direction, β_y, does not have a big influence on the brilliance of the undulator radiation.

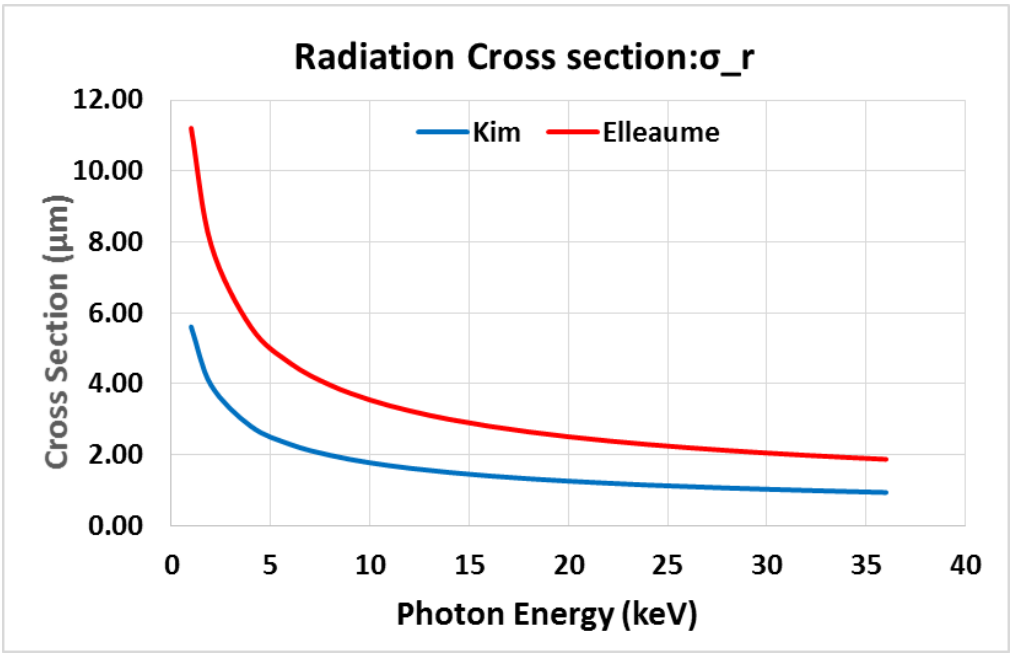

Fig. 4.2: Dependence of the radiation cross-section on the undulator photon energy (according to [4.8] and [4.15]).

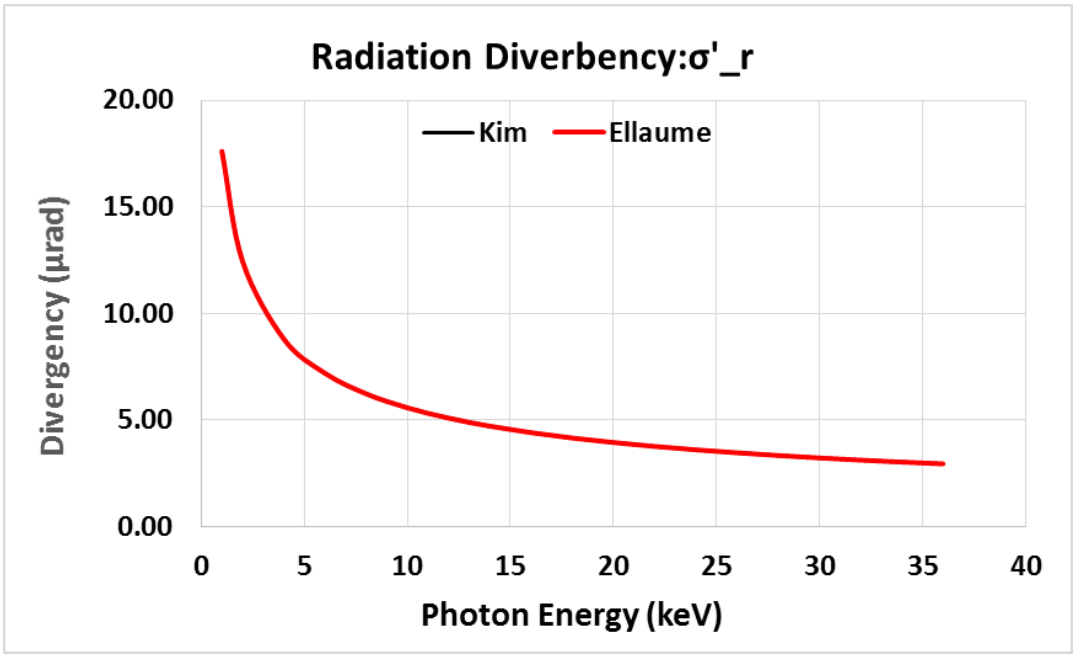

Fig. 4.3: Dependence of the radiation divergence on the undulator photon energy

The emittance ε_r of synchrotron radiation from the insertion devices is $\sigma_r \sigma_r'$, and the corresponding plot is displayed in Fig. 4.4.

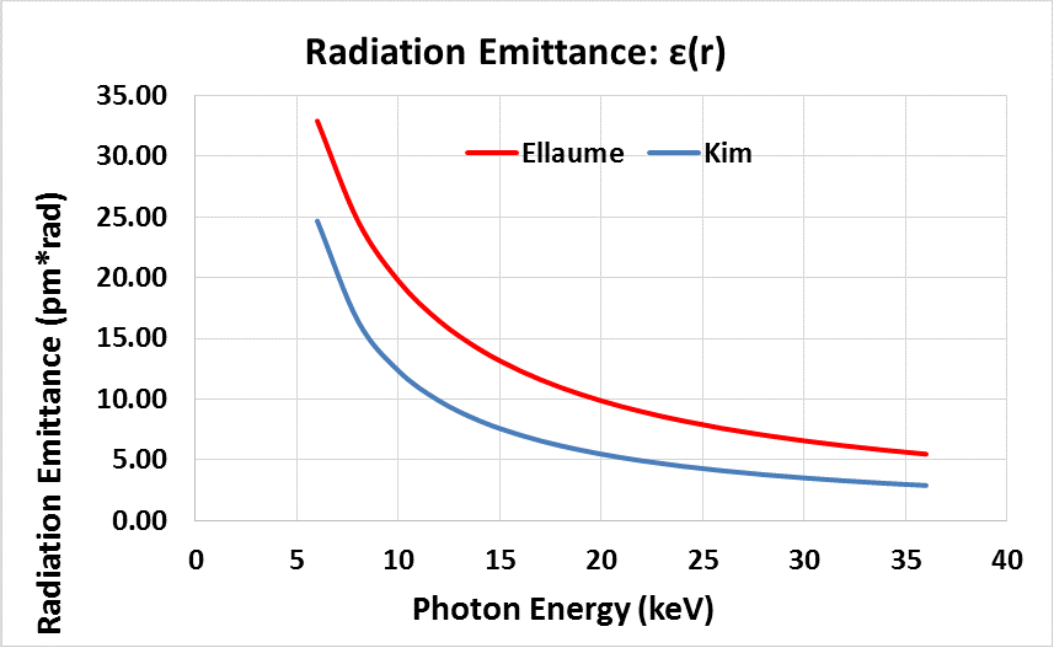

Fig. 4.4: Dependence of the synchrotron radiation emittance on the photon energy

The photon energy E_r of the undulator is proportional to the square of the beam energy and the harmonic number n; see Eqs. (4.11) and (4.12). It is inversely proportional to the undulator period λ_u and a function of the undulator parameter K. Hence, by increasing beam energy from 2.5 to 3 GeV, the photon energy will be increased by a factor of 1.44.

This investigation shows that the emittance of the photon beam in the whole energy range is smaller than 30 pmrad. The emittance of the SEE-LS should be around 250 pmrad; hence, for the brilliance calculations the photon emittance does not have any influence. To achieve a high brilliance the cross-section of the stored electron beam has to be minimized, and this has to be done by decreasing the emittance as well the beta functions.

4.4 Lattice for the SEE-LS

Well-known lattices for the 4th generation light sources are: a) the 7MBA lattice used for MAX IV [4.16]; b) the 5 multi-bend achromat (5MBA) used for SIRIUS [4.17]; c) the HMBA lattice used for the upgrade of ESRF and other light sources [4.18, 4.19]; d) the double double-bend achromat (DDBA) and double triple-bend achromat (DTBA) lattices used for a possible upgrade of Diamond [4.20, 4.21]; e) the S6BA (also a DTBA) used for the upgrade of ELETTRA [4.22]; and f) the 7MBA lattice with anti-bends and longitudinal gradients in the magnets [4.23] proposed for the upgrade of SLS. Recently, a possible lattice for the upgrade of SOLEIL was presented [4.24]. The lattice file of SOLEIL is not available at present, and the lattice file used was extracted from the plots of the beta functions. The specifications of all these lattices are summarized in Table 4.1.

The DDBA, DTBA, and S6BA lattices have the advantage of containing an additional straight section in the middle of the achromat. These straight sections can be used to install small insertion devices and all the instrumentation needed for operation of the machine; hence, more space is available for users. This is reflected in the percentage of the circumference devoted to straight sections. The HMBA lattice has the requirement that the phase advance between the dispersion regions must be π (vertical) or 3π (horizontal). This limits the settings for the smallest emittance but reduces the number of sextupoles needed. The specifications, according to a matching for a circumference of roughly 350 m, are given in Table 4.2.

Table 4.1: Parameters of the 4th generation light source lattices proposed for the upgrade of the facilities

Lattice	MAX IV	HMBA	SIRIUS	DDBA	DTBA	S6BA	SLS-2	SOLEIL-2
Circumference (m)	528	506.28	518.4	561	561	259.2	290.4	354.7
Period	20	22	20	24	24	12	12	20
Achromat-length (m)	26.4	23.013	25.92	23.37	23.37	21.6	24.2	17.73
Energy (GeV)	3	3	3	3	3	2	2.4	2.75
Emittance (pmrad)	328	141	250	272	101	255	102	72
Tune Q_x	44.06	53.6	48.1	51.21	57.45	33.1	37.2	55.2
Tune Q_y	17.76	15.43	13.17	17.31	20.36	9.2	15.3	18.2
Chromaticity ξ_x	−51.47	−87.86	−124.4	−129	−78.15	−75	−95	−134
Chromaticity ξ_y	−51.37	−70.78	−79.9	−93.51	−109.7	−51	−35.2	−125

From the relation that the emittance is proportional to the square of the energy and inversely proportional to the cube of the number of magnets, it is possible to estimate the emittance for this lattice with a circumference of roughly 350 m. Accordingly, lattice files for the matched achromats have been evaluated. The corresponding lattices are presented in Figs. 4.5–4.14

Given the requirements for the circumference, emittance, and number of straight sections, only the HMBA, DTBA, S6BA, and SLS-2 lattices can be taken as candidates for the SEE-LS. Consideration of nonlinear beam-dynamic issues eventually favoured the HMBA and the S6BA. Finally, owing to the reduced numbers of sextupoles and the larger dynamic aperture, the HMBA lattice was chosen as the candidate lattice for the SEE-LS. However, the S6BA lattice is also promising. In making a final decision, and considering the further calculations which have to be done, another lattice solution such as the proposed SOLEIL upgrade cannot be excluded in this case.

4.4.1 The 7MBA lattice

The 7MBA lattice (Fig. 4.5) is built with five unit cells, as shown in Fig. 4.6, and two matching sections. The lattice functions within each unit cell are like a TME structure and those in the matching cell are like a DBA structure (see Fig. 4.1). With a period of $N = 14$ the circumference is roughly 409 m, leading to an emittance of 288 pmrad. In order to reach a circumference of roughly 350 m, the number of achromats has to be reduced to 12, which leads to an emittance of roughly 460 pmrad. In addition, the horizontal chromaticity is quite high, which should reduce the dynamic aperture. Because of this, using large numbers of 7MBA lattices is not an attractive solution for the SEE-LS.

Table 4.2: Parameters of the 4th generation light source lattices that are candidates for the SEE-LS with a circumference of roughly 350 m.

Lattice	7MBA	HMBA I	HMBA II	SIRIUS	DTBA	S6BA	SLS-2	SOLEIL-2
Energy (GeV)	3	3	2.5	3	3	2.5	3	2.75
Circumference (m)	408.9	345.4	329.2	362	361.8	347.2	332.4	354.7
Emittance (pmrad)	288	255	218	806	365	166	131	72
Period	14	16	16	14	16	16	14	20
Tune Q_x	45.23	41.38	37.2	31.39	39.24	44.18	43.29	64.4
Tune Q_y	12.41	12.26	12.22	10.39	13.22	12.39	10.92	22.3
Chromaticity ξ_x	−128.9	−104.73	−79.27	−97.4	−59.1	−109	−79.87	−157
Chromaticity ξ_y	−46.74	−70.58	−60.26	−37.97	−73	−82.4	−38.36	−127
U_o (keV)	609	484	280	494	510	310	1131	340
J_x	1.34	1.71	1.86	1.43	1.46	1.45	1.7	1.71
$\sigma_x(0)$ (μm)	56.1	70.9	55.8	131.4	45.7	44	19.4	8.5
$\sigma_y(0)$ (μm)	5.4	2.8	3.4	6	3.9	3.2	6.3	2.2
$\sigma'_x(0)$ (μrad)	5.1	3.6	3.9	6.13	8	3.8	6.8	8.5
$\sigma'_y(0)$ (μrad)	0.92	1.76	1.48	0.83	1.29	1.53	0.8	2.24
Area (μm^2)	302.94	198.52	189.72	788.4	178.23	140.8	122.22	18.7
Percentage	17.9	26.1	27.4	27.1	37.5	31.7	22.3	25

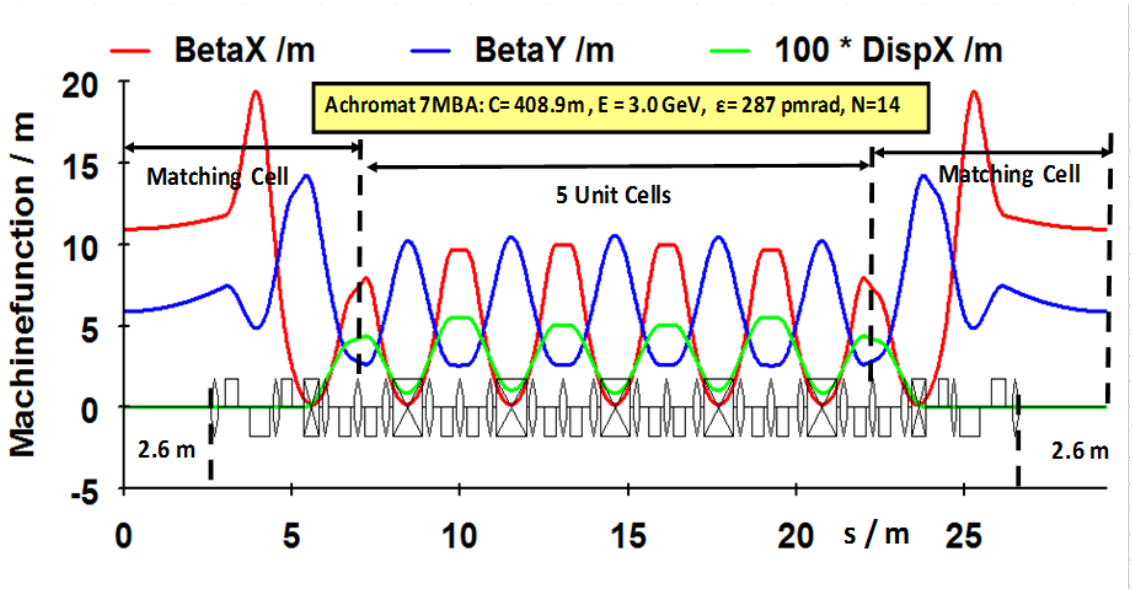

Fig. 4.5: The machine functions of a 3 GeV-7MBA lattice (like MAX IV)

4.4.2 The 3 GeV HMBA I lattice

Completely different from the 7MBA lattice is the HMBA lattice (see Fig. 4.7) as proposed for the upgrade of the ESRF [4.18, 4.19]. The lattice consists of two DBA structures for the matching to the straight sections and a matching section in the middle of the arc (see Fig. 4.7). To reduce the number of sextupoles, the phase advance between the two DBA structures has to be $\Delta\phi(x) = 3\pi$ and $\Delta\phi(y) = \pi$; this places some limitations on the selection of the working points (tunes). With a period of $N = 16$ and an energy of 3 GeV, the circumference is 345.4 m, leading to an emittance of 255 pmrad. The horizontal chromaticity is also quite high, but a first dynamic aperture calculation has shown that an acceptable value can be reached, which could be a solution. For the installation of the injection, the RF system,

and machine components, up to four straight sections are needed; hence, for the installation of insertion devices there should be 12 straight sections, whereas for the 7MBA only 10 straight sections are available to the user. This is a big advantage of the HMBA over the 7MBA lattice.

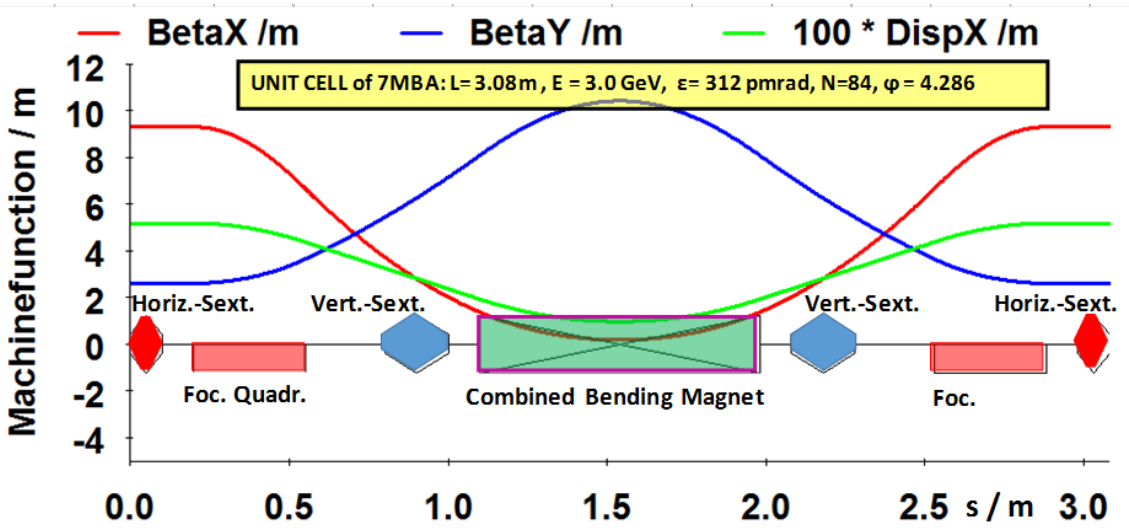

Fig. 4.6: The arrangements of magnets and the machine functions of a 3 GeV unit cell of the 7MBA lattice

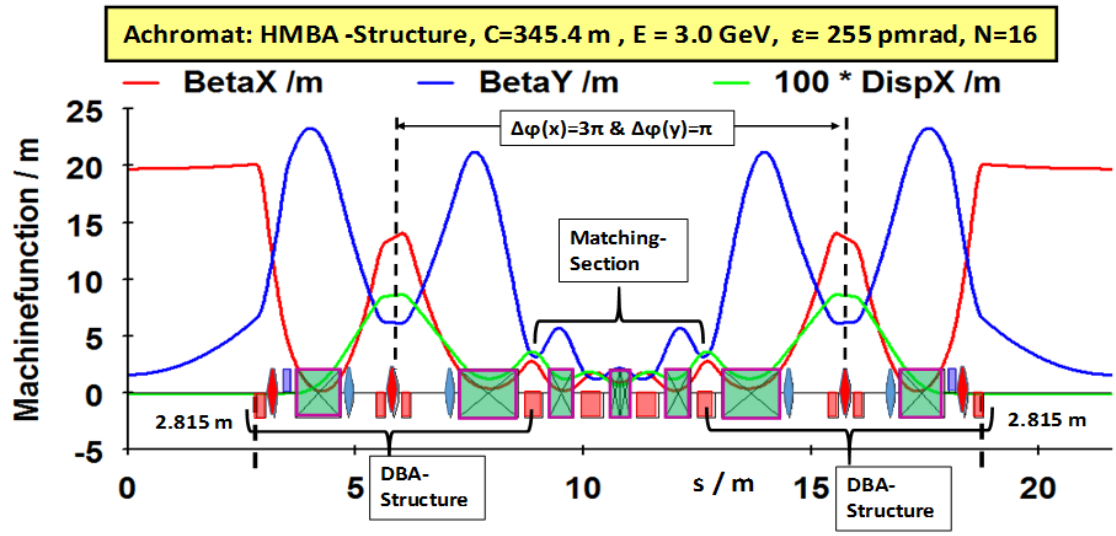

Fig. 4.7: The machine functions of a 3 GeV HMBA I lattice (like ESRF-EBS)

4.4.3 The 2.5 GeV HMBA II lattice

In order to see the difference in the energy, the 3 GeV version was also matched to an energy of 2.5 GeV (see Fig. 4.8). Accordingly, the emittance reduces to 218 pmrad and the circumference goes down to 329.2 m. According to the scaling of the emittance with the energy, the emittance of the HMBA I lattice should go down to 177 pmrad for 2.5 GeV. Hence there is still some room for optimization. The length of the straight section is 5.63 m. This lattice could be a solution for the design of the SEE-LS. A further advantage of the 2.5 GeV version is that the radiated energy per turn decreases by a factor of around 2 (from 484 to 280 keV—see U_0 in Table 4.2); this reduces the cost of the RF system.

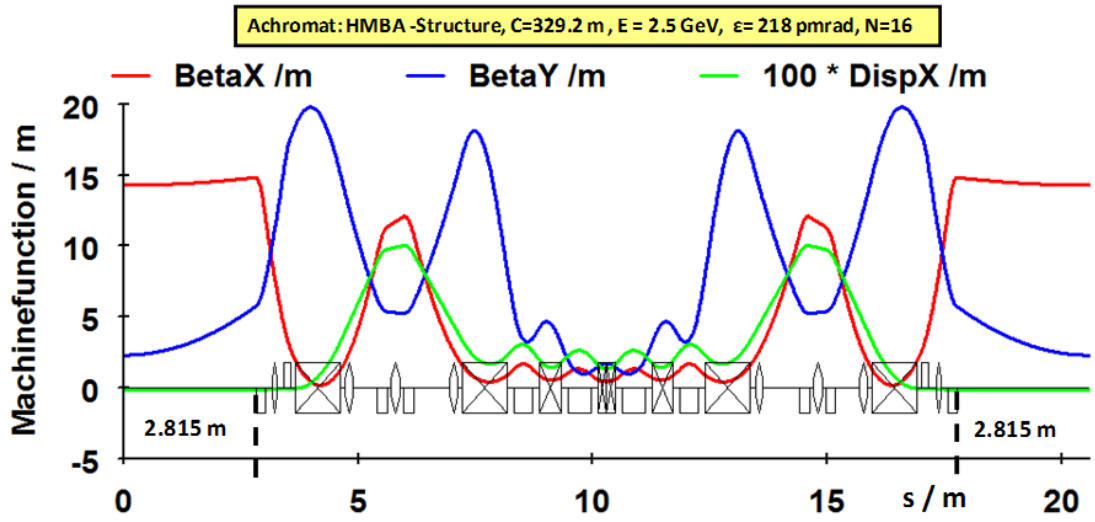

Fig. 4.8: The machine functions of a 2.5 GeV HMBA II lattice (like ESRF-EBS)

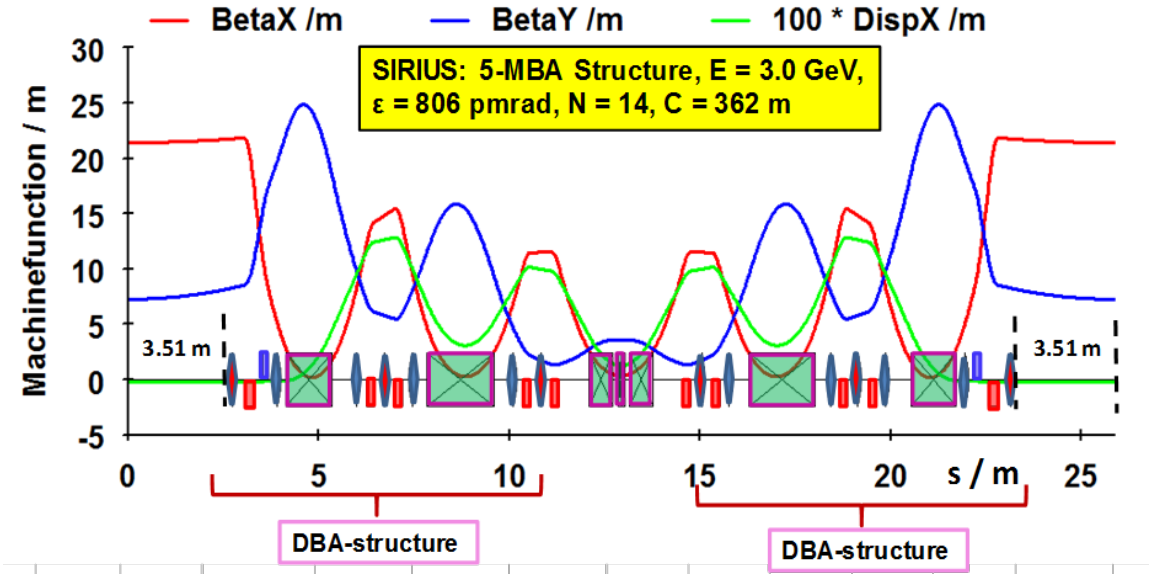

Fig. 4.9: The machine functions of a 3 GeV 5MBA lattice (like SIRIUS II)

4.4.4 The 3 GeV 5MBA lattice

The 5MBA lattice of SIRIUS, matched to a circumference of roughly 350 m, is presented in Fig. 4.9. The structure of the 5MBA is roughly the same as that of the HMBA (see above), except that the matching of the two matching cells will be done by only one bending magnet. With a circumference of 362 m and a period of $N = 14$, an emittance of 806 pmrad could be reached. The scaling of the original SIRIUS lattice with an emittance of 250 pmrad and $N = 20$ would result in an emittance of roughly 730 pmrad, so there is still some room for optimization. Nevertheless, because of the high emittance and the relative low number of straight sections available to the user, this lattice is not a good candidate for the SEE-LS.

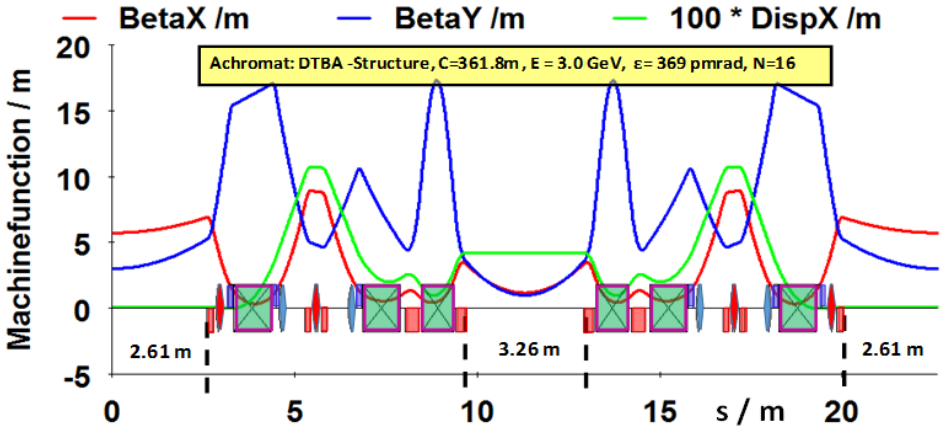

Fig. 4.10: The machine functions of a 3 GeV DTBA lattice (like the upgrade of Diamond)

4.4.5 The 3 GeV DTBA lattice

This lattice (see Fig. 4.10) yields a relatively large emittance of 365 pmrad with a circumference of 361.8 m. As for the other lattices, the period is $N = 16$. Also, the phase advance between the two DBA structures has to be $\Delta\phi(x) = 3\pi$ and $\Delta\phi(y) = \pi$. The advantage of this lattice is the additional straight section in the middle of the arc. This straight section can be used for the installation of the RF system as well as other machine components. Because of the relatively large emittance and circumference, this is not considered a candidate lattice for the SEE-LS.

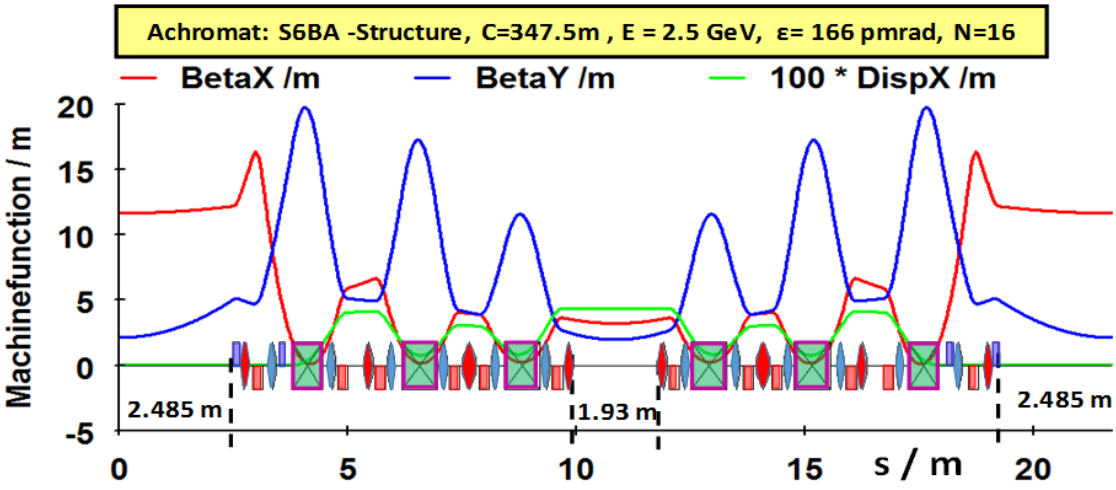

Fig. 4.11: The machine functions of a 2.5 GeV S6BA lattice (like the upgrade of ELETTRA)

4.4.6 The 2.5 GeV S6BA lattice

This lattice (see Fig. 4.11) leads to a circumference of 347.2 m and an emittance of 166 pmrad for an energy of 2.5 GeV, which in comparison with the other lattices is fairly low [4.25]. As for the other lattices, the period is $N = 16$. Like the DTBA lattice, the S6BA has the advantage of having an additional straight section in the middle of the arc. The chromaticities are rather high, but initial calculations have shown that a sufficient dynamic aperture should be attainable. This is so far a very good solution, if an energy of 3 GeV is not needed. Because there is no condition on the phase advance, the number of sextupoles is relatively high, but the flexibility in choosing the tune values is high as well.

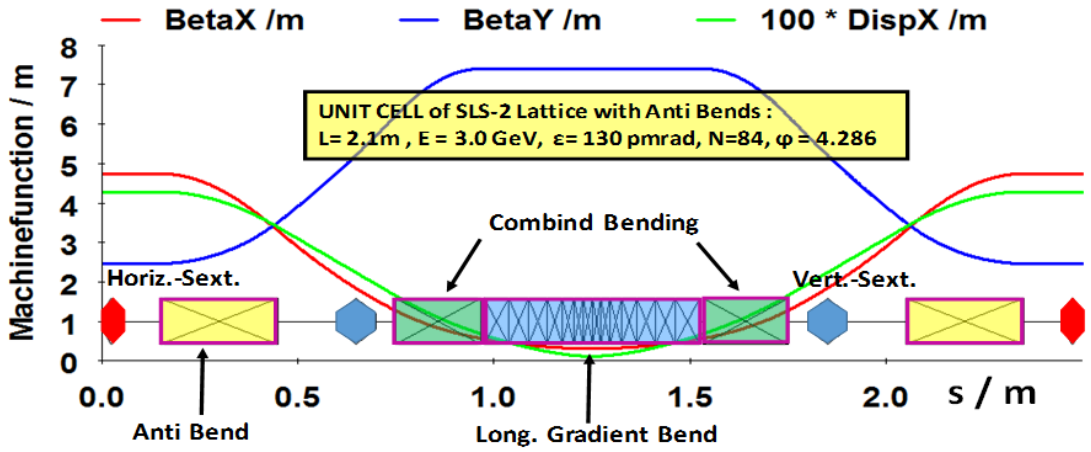

Fig. 4.12: The machine functions within the unit cell of the 3 GeV lattice proposed for the upgrade of SLS

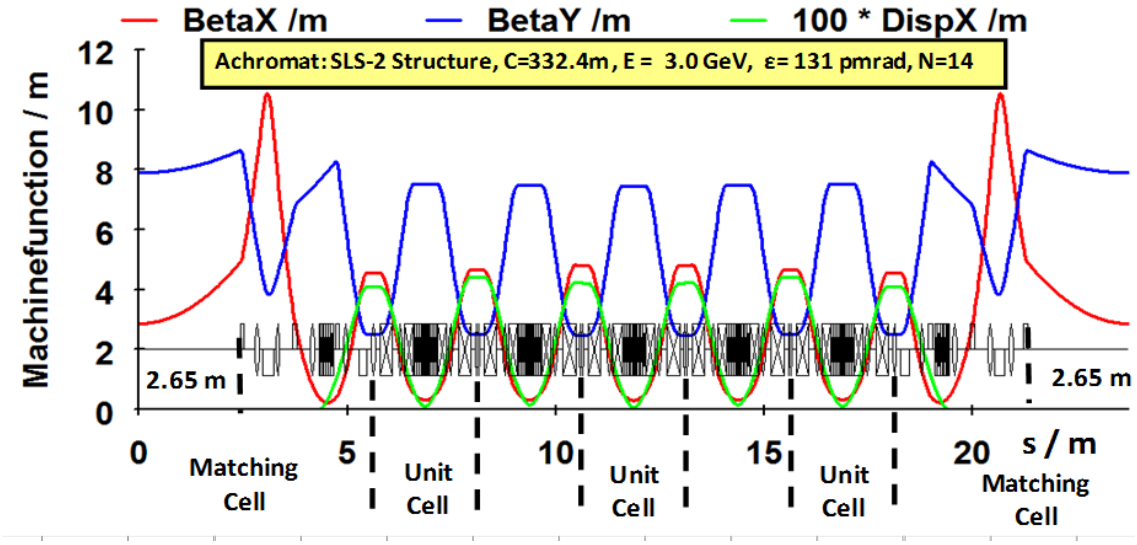

Fig. 4.13: The machine functions of the 3 GeV lattice proposed for the upgrade of SLS

4.4.7 The 3 GeV SLS-2 lattice

For the upgrade of the SLS, a 7MBA lattice will also be used. There is, however, a big difference between the lattice of its unit cell and that of MAX IV (compare Figs. 4.12 and 4.6): instead of using a quadrupole at the beginning of the unit cell, a so-called 'anti-bend' will be used. An anti-bend [4.23] is a shifted quadrupole and reflects the beam to the outer side of the ring; hence the anti-bend has a focusing as well as a deflection effect. The consequences for the machine function can be seen by comparing Figs. 4.6 and 4.12. In Fig. 4.6 the dispersion function has values of around 2 cm, whereas in Fig. 4.12 it has a value of more or less 0 cm. Also, the horizontal beta function has smaller values with the anti-bends in the middle of the bend, with 768,ing. Both effects decrease the emittance by a lot.

In addition to using the anti-bend, the emittance is reduced by means of a longitudinal gradient bending magnet, in which the magnetic field goes up to 2.5 T. The introduction of the longitudinal gradient and the anti-bend greatly reduces the emittance; the emittance of the unit cell decreases from 349 to 144 pmrad. The anti-bend and the longitudinal gradient both change the emittance by a factor of 1.5; for an energy of 2.5 GeV the emittance would go down to roughly 90 pmrad. However, the magnets are very complicated to build, and first dynamic aperture calculations have yielded a relatively small value. With a period of $N = 14$, the available straight sections are a bit smaller than in other lattices. Because of its complexity, small dynamic aperture, and reduced number of straight sections, the SLS-2 lattice will not be considered as a candidate for the SEE-LS.

4.4.8 The 2.75 GeV SOLEIL-2 lattice

For the upgrade of SOLEIL, the proposed lattice is shown in Fig. 4.14. The lattice file is not officially available, so the editor generated the file from different plots [4.24, 4.26] presented at various workshops and conferences. It is more or less an HMBA lattice as for the upgrade of the ESRF. A new element is the incorporation of anti-bends to reduce the emittance further. With the length of the achromat being roughly 17.5 m, it is a very compact design; therefore it is possible to obtain a period of $N = 20$ with a circumference of 353.1 m. Because the final design is not finished, this lattice will not be considered as a solution for the SEE-LS.

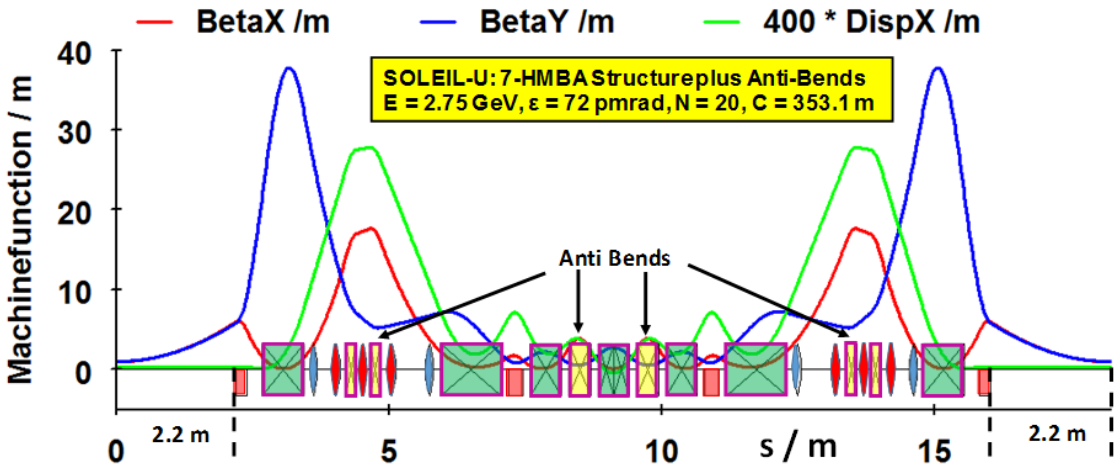

Fig. 4.14: The machine functions of the 2.75 GeV lattice proposed for the upgrade of SOLEIL

4.4.9 Number of magnets

One factor for the budget is the number of components and, in this case, the number of magnets. The different lattices discussed here require the following numbers of magnets.

- **7MBA**: 98 bending magnets, 252 quadrupoles, and 308 sextupoles; a total of 658 magnets
- **HMBA**: 112 bending magnets, 160 quadrupoles, and 128 sextupoles; a total of 400 magnets
- **SIRIUS**: 70 bending magnets, 168 quadrupoles, and 196 sextupoles; a total of 434 magnets
- **DTBA**: 96 bending magnets, 256 quadrupoles, and 128 sextupoles; a total of 480 magnets
- **S6BA**: 96 bending magnets, 256 quadrupoles, and 288 sextupoles; a total of 640 magnets
- **SLS-2**: 272 bending magnets, 160 quadrupoles, and 336 sextupoles; a total of 768 magnets
- **SOLEIL-2:** 140 bending magnets, 200 quadrupoles, and 200 sextupoles; a total of 540 magnets.

The SLS-2 lattice has the largest number (768) and the HMBA the smallest number (400) of magnets.

4.5 Brilliance calculations

Brilliance calculations have been done for a *cryogenic permanent magnet undulator* (CPMU) with a period length of 16 mm and a beam current of 500 mA. The detailed parameters of the insertion device are given in Table 4.3, in which ε_n^{th} denotes the photon energy of the nth harmonic.

Table 4.3: Data for the CPMU 16 used for the brilliance calculations

Parameter	Value	Value	Unit
Energy	3	2.5	GeV
Gap value	4.2	4.2	mm
B_0	1.26	1.26	T
Total length	2	2	m
Period length (λ_0)	16	16	mm
Number of periods	125	125	
K value	1.88	1.88	
λ_1	0.00	0.00	µm
σ_r	5.71	6.85	µm
$\boldsymbol{\sigma}_r'$	12.68	15.22	µrad
ε_1^{st}	1.93	1.34	keV
ε_3^{rd}	5.78	4.02	keV
ε_5^{th}	9.64	6.69	keV
ε_7^{th}	13.49	9.37	keV
ε_9^{th}	17.35	12.05	keV
ε_11^{th}	21.20	14.72	keV

The brilliances for the 3 GeV HMBA, 2.5 GeV HMBA, 2.5 GeV S6BA, and 3 GeV MAX IV lattices are presented in Fig. 4.15 for harmonic numbers up to $n = 9$. The maximum brilliance is in the range of 3×10^{21} photons/s/mm^2/rad^2/0.1%BW for the soft-X-ray region and goes up to 1×10^{18} photons/s/mm^2/rad^2/0.1%BW for the hard X-ray region (35 keV photon energy). In order to exhibit the differences between a 3 GeV and a 2.5 GeV electron beam, the corresponding brilliances are plotted in Fig. 4.16. Going from 2.5 GeV to 3 GeV, the brilliance will increase by photon energies of roughly 10 keV.

The brilliances of the different lattices for different photon energies are summarized in Table 4.4. In general there are not great differences between the different lattices. This was already explained in chapter 1 and is due to the large contribution of the undulator radiation. Owing to the small emittance of SLS-2, this lattice provides the highest brilliance, greater by around a factor of 2 than the others.

For a beam energy of 2.5 GeV, the brilliances of up to 10 keV are roughly the same as for 3 GeV. For photon energies of roughly 15 keV, the brilliance is smaller by approximately a factor of 2, and for 20 keV it is smaller by a factor of 10 for a beam energy of 2.5 GeV. For photon energies as high as 20 keV, the brilliance at 2.5 GeV is more than one order of magnitude smaller in comparison to a 3 GeV machine (see Fig. 4.16).

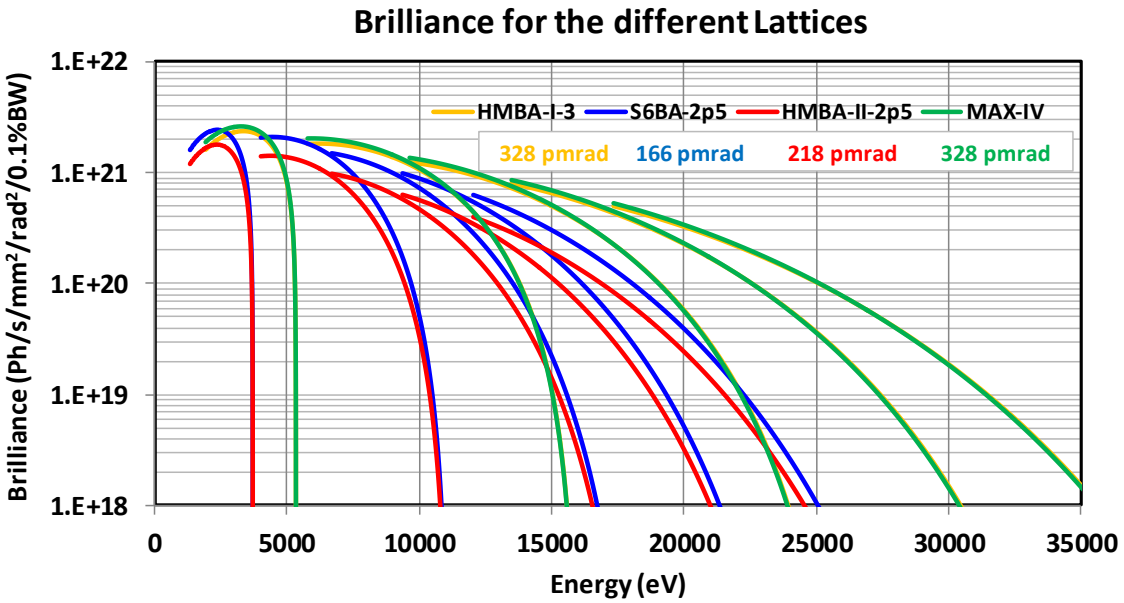

Fig. 4.15: Brilliances of the insertion device CPMU 16 for the 3 GeV HMBA, 2.5 GeV HMBA, 2.5 GeV S6BA, and 3 GeV MAX IV lattices.

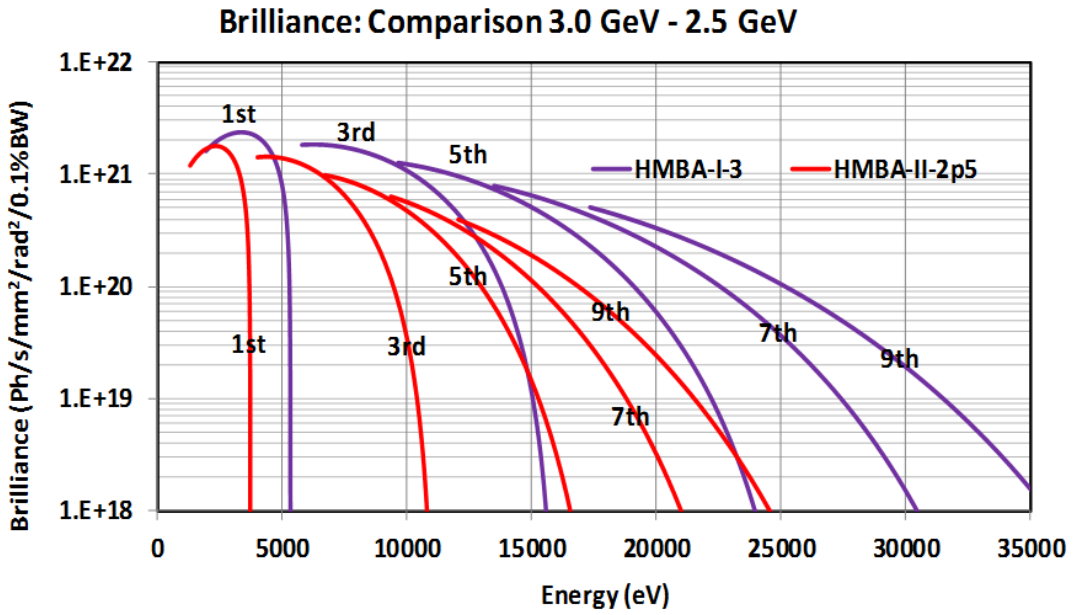

Fig. 4.16: Brilliances of the insertion device CPMU 16 for the 3 GeV HMBA and 2.5 GeV HMBA lattices

Table 4.4: Brilliances in photons/(s mm^2 mrad^2 0.1BW) of the various lattices for different photon energies in keV.

Lattice	Energy	5 keV	10 keV	15 keV	20 keV	25 keV	30 keV
MAX IV	3 GeV	3.70E+21	2.60E+21	1.45E+21	6.50E+20	2.00E+20	3.00E+19
7MBA	3 GeV	2.50E+21	1.70E+21	9.50E+20	4.50E+20	1.40E+20	2.10E+19
HMBA	3 GeV	3.40E+21	2.60E+21	1.50E+21	7.30E+20	2.20E+20	3.60E+19
DTBA	3 GeV	3.20E+21	2.00E+21	1.10E+21	4.60E+20	1.30E+20	1.90E+19
SLS-2	3 GeV	5.20E+21	3.90E+21	2.05E+21	9.90E+20	3.00E+20	5.00E+19
HMBA	2.5 GeV	2.70E+21	1.40E+21	4.40E+20	5.40E+19		
S6BA	2.5 GeV	3.90E+21	2.10E+21	7.00E+20	8.50E+19		

As mentioned in section 4.4, the brilliance is a function of the beam cross-section, given by the beta function. The dependence of the brilliance on the beta functions is presented in Table 4.5. At lower photon energies, the brilliance increases by roughly a factor of 2 for smaller beta functions, but at higher photon energies the brilliance goes through a maximum around beta function values of 5–10 m/rad. This is more clearly seen in Table 4.6, in which the brilliances are normalized so that the values corresponding to the largest beta function become 1.

Table 4.5: Brilliances of the 3 GeV HMBA lattice for different beta functions and photon energies in keV

Beta value	5 keV	10 keV	15 keV	20 keV	25 keV	30 keV
19.73	3.40E+21	2.60E+21	1.50E+21	7.30E+20	2.20E+20	3.60E+19
15	4.00E+21	3.20E+21	1.90E+21	8.50E+20	2.70E+20	4.20E+19
10	4.60E+21	3.60E+21	2.05E+21	9.50E+20	2.90E+20	4.60E+19
5	6.00E+21	4.40E+21	2.40E+21	1.05E+21	3.00E+20	4.70E+19
2.5	7.20E+21	4.80E+21	2.50E+21	1.00E+21	2.60E+20	3.70E+19
1.61	7.50E+21	4.30E+21	2.20E+21	8.50E+20	2.00E+20	2.90E+19

Table 4.6: Normalized brilliances of the 3 GeV HMBA lattice for different beta functions

Beta value	5 keV	10 keV	15 keV	20 keV	25 keV	30 keV
19.73	1.00	1.00	1.00	1.00	1.00	1.00
15	1.18	1.23	1.27	1.16	1.23	1.10
10	1.35	1.38	1.37	1.30	1.32	1.28
5	1.76	1.69	1.60	1.44	1.36	1.31
2.5	2.12	1.85	1.67	1.37	1.18	1.03
1.61	2.21	1.65	1.47	1.16	0.91	0.81

4.6 Summary

Based on the given emittance of 131 pmrad, the SLS-2 lattice seems the most favourable one, but the machine is complex, the dynamic aperture is small, and the costs will be higher than for the other lattices. This lattice also has a large number of magnets and is perhaps not the best solution for the SEE-LS.

Next comes the 6SBA lattice, with a relatively small emittance of 166 pmrad at 2.5 GeV and an additional straight section in the middle of the arc. Initial calculations for the dynamic aperture show promising results. This lattice could be suitable for the SEE-LS, but it still has to be optimized.

The 3 GeV HMBA I and 2.5 GeV HMBA II lattices are possible solutions too.

The DTBA lattice can achieve a fairly large emittance, but its main advantage is the additional straight section in the middle of the arc.

The 7MBA lattice is not attractive because of the larger emittance, larger circumference, and reduced period.

The emittance and the brilliance are not the only relevant factors in choosing the lattice type. One also has to look at the overall cost of the project. A main part of the cost comes from the RF system and is determined by the radiation loss per turn, U_o. For the 2.5 GeV machines (see Table 1) U_o is at least a factor of 2 smaller than for the 3 GeV machines. Hence one could start with a 2.5 GeV version and later upgrade to 3 GeV.

The 3 GeV HMBA I lattice scaled to an energy of 2.5 GeV results in an emittance of 177 pmrad. The difference in length between the two solutions at 3 GeV and 2.5 GeV is only 16.2 m, which is insignificant. Hence, for the first proposal of a lattice for the SEE-LS, the 3 GeV HMBA I lattice operating at an energy of 2.5 GeV should be used.

At present the SOLEIL-2 lattice cannot be used as a proposal for the SEE-LS because the details of the lattice are not known. At the 6th Diffraction Limited Storage Ring (DLSR) Workshop held at the Lawrence Berkeley National Laboratory, some more lattices were presented with much better results.

Using an HMBA lattice for the first proposal has the further advantage that many components from the ESRF-EBS upgrade can be used.

References

[4.1] D. Einfeld and M. Plesko, Design of a diffraction limited light source, Proc. SPIE Electron-Beam Sources of High-Brightness Radiation, San Diego, California, USA, 29 November 1993. https://doi.org/10.1117/12.164802

[4.2] D. Einfeld and M. Plesko, *Nucl. Instrum. Methods Phys. Res. A* **335** (1993), 402, https://doi.org/10.1016/0168-9002(93)91224-B

[4.3] D. Einfeld, J. Schaper, and M. Plesko, Design of a diffraction limited light source (DIFL), Proc. 10th ICFA Beam Dynamics Panel Workshop: 4th Generation Light Sources, Grenoble, France, 22–25 January 1996. http://doi.org/10.5281/zenodo.2671721

[4.4] D. Einfeld, J. Schaper, and M. Plesko, Design of a diffraction limited light source (DIFL), Proc. Particle Accelerator Conference, Dallas, Texas, USA, 1–5 May 1995, p. 177. https://doi.org/10.1109/PAC.1995.504602

[4.5] D. Einfeld, J. Schaper, and M. Plesko, *J. Synchrotron Rad.* **21** (2014) 856, https://doi.org/10.1107/S160057751401193X

[4.6] P.F. Tavares *et al.*, *J. Synchrotron Rad.* **25** (2018) 1291, https://doi.org/10.1107/S1600577518008111

[4.7] R. Coisson, *Opt. Eng.* **27** (1988) 273250, https://doi.org/10.1117/12.7977923

[4.8] H. Onuki and P. Elleaume (eds.), *Undulators, Wigglers and Their Applications* (Taylor & Francis, New York, 2003), https://doi.org/10.4324/9780203218235

[4.9] A. Ropert, Lattices and emittances, CAS-CERN Accelerator School: Synchrotron Radiation and Free Electron Lasers, Grenoble, France, 22–27 April 1996, CERN-1998-004 (CERN, Geneva, 1998), p. 91. http://dx.doi.org/10.5170/CERN-1998-004.91

[4.10] R. Chasman, K. Green, and E.M. Rowe, *IEEE Trans. Nucl. Sci.* **22** (1975) 1765, https://doi.org/10.1109/TNS.1975.4327987

[4.11] D. Einfeld and G. Muelhaupt, *Nucl. Instrum. Methods* **172** (1980) 55, https://doi.org/10.1016/0029-554X(80)90607-2

[4.12] M. Sommer, Optimization of the emittance of electron storage rings, Report LAL/RT/83-15 (Laboratoire de l'Accélérateur Linéaire, Orsay, 1983), http://inspirehep.net/record/195918

[4.13] G. Wüstefeld, The minimization of the natural emittance in the triple bend achromat, Report BESSY TB 108/87 (March 1987).

[4.14] R. Nagaoka and A.F. Wrulich, Emittance minimisation with longitudinal dipole field variation, *Nucl. Instrum. Methods Phys. Res. A* **575** (2007) 292, https://doi.org/10.1016/j.nima.2007.02.086

[4.15] K.-J. Kim, Characteristics of synchrotron radiation, AIP Conf. Proc. **184** (1989) 565, https://doi.org/10.1063/1.38046

[4.16] S.C. Leemann, Recent improvements to the lattices for the MAX IV storage rings, Proc. IPAC2011, San Sebastián, Spain, 4–9 September 2011, p. 3029. http://accelconf.web.cern.ch/AccelConf/IPAC2011/papers/thpc059.pdf

[4.17] L. Liu *et al.*, A new 5BA low emittance lattice for Sirius, Proc. IPAC2013, Shanghai, China, 12–17 May 2013, p. 1874. https://inspirehep.net/record/1338708

[4.18] J.L. Revol *et al.*, ESRF upgrade phase II, Proc. IPAC2013, Shanghai, China, 12–17 May 2013, p. 1140. https://inspirehep.net/record/1337024

[4.19] S. Liuzzo *et al.*, Hybrid multi bend achromat at 3 GeV for future 4th generation light sources, Proc. IPAC2016, Busan, Korea, 8–13 May 2016, p. 2822. https://doi.org/10.18429/JACoW-IPAC2016-WEPOW006

[4.20] R. Bartolini *et al.*, Novel lattice upgrade studies for Diamond light source, Proc. IPAC2013, Shanghai, China, 12–17 May 2013, p. 240. https://inspirehep.net/record/1336784

[4.21] R. Bartolini, Design and optimisation of nonlinear dynamics in diffraction-limited synchrotron light sources, Proc. IPAC2016, Busan, Korea, 8–13 May, 2016, p. 33. https://doi.org/ 10.18429/JACoW-IPAC2016-MOZA02

[4.22] E. Karantzoulis *et al*., Status of Elettra and future upgrade, Proc. IPAC2018, Vancouver, Canada, 29 April – 4 May 2018, p. 4054. https://doi.org/10.18429/JACoW-IPAC2018-THPMF010

[4.23] A. Streun, *Nucl. Instrum. Methods Phys. Res. A* **737** (2014) 148, https://doi.org/10.1016/j.nima.2013.11.064

[4.24] A. Loulerge *et al*., Baseline lattice for the upgrade of Soleil, Proc. IPAC2018, Vancouver, Canada, 29 April – 4 May 2018, p. 4726. https://doi.org/10.18429/JACoW-IPAC2018-THPML034

[4.25] E. Karantzoulis, Overview of the ELETTRA 2.0 project, 6th DLSR Workshop, Lawrence Berkeley National Laboratory, 29–31 October 2018. https://web.archive.org/web/20190515084118/https://drive.google.com/file/d/1rQNFApCusRtNNV40qaDVhwJgMt1ul8YQ/view

[4.26] L. Nadolski, Progress report of the lattice studies for the SOLEIL upgrade, 6th DLSR Workshop, Lawrence Berkeley National Laboratory, 29–31 October 2018. https://web.archive.org/web/20190515084525/https://drive.google.com/file/d/1Dnq9h9-yMTaEVpvJH_iaZsjTCnSpGxGe/view